scientific reports

Check for updates

OPEN

Solving the Richards infiltration equation by coupling physics-informed neural networks with Hydrus-1D

Yanling Li[1], Qianxing Sun[1]✉, Yuliang Fu[2]✉ & Junfang Wei[3]

The movement and infiltration of groundwater play a crucial role in environmental engineering and water resource management. The Richards equation, a fundamental model describing water flow in unsaturated soils, encounters significant challenges in traditional numerical solutions due to its strong nonlinearity, complex boundary conditions, and computational inefficiency. To address these issues, this study proposes an improved physics-informed neural network (PINN) method based on data fusion. This approach is designed to handle the intricate boundary conditions and nonlinear water diffusion characteristics in groundwater seepage by integrating data with physical constraints, thereby forming a dual-driven solution framework that leverages both data and physics. The proposed improved algorithm integrates Hydrus data, leveraging a small portion of data to reduce the model's dependence on parameter initialization. Simultaneously, it enables the model to automatically adjust to variations in physical processes under different data conditions, thereby enhancing the accuracy and stability of the solution. Comparaison with experimental results demonstrates the strong generalization ability of this method, particularly in data-scarce regions, where physical constraints ensure the reliability of the model's solutions.

Keywords Richards equation, PINN algorithm, Hydrus-1D, Dual-driven model

In science and engineering, solving partial differential equations (PDEs) is a critical yet challenging task. Among them, The Richards equation, which governs flow in saturated–unsaturated porous media[1], is strongly nonlinear and prone to numerical instability under heterogeneous boundary conditions. Traditional methods such as finite element method often suffer from slow convergence or high computational cost, limiting their efficiency in complex, multi-scale hydrological settings[2]. In recent years, machine learning techniques, particularly deep learning, have achieved groundbreaking advancements across various fields[3]. However, traditional machine learning algorithms primarily rely on feeding large amounts of data into models for self-learning and automation, with limited incorporation of prior knowledge. This deficiency results in reduced interpretability, limited generalization capability, and constrained extrapolation performance to some extent[4]. This limitation is particularly pronounced in data-scarce and complex domains, such as groundwater seepage and runoff simulation, where hydrological models require long-term monitoring data. In remote areas or developing countries, historical hydrological data are often scarce, making it challenging for data-driven approaches to effectively predict water resource variations[5,6]. Therefore, there is an urgent need for a more efficient and flexible solution that reduces dependence on extensive data while enhancing the model's generalization ability and interpretability under heterogeneous infiltration conditions. Such an approach should achieve the synergistic optimization of physical laws and data-driven features.

Raisi et al.[7] proposed the physics-informed neural network (PINN) algorithm, which innovatively integrates the advantages of data-driven machine learning and physics-based modeling. PINNs leverage the powerful representation capability of neural networks along with the physical knowledge of PDEs, approximating PDE solutions through neural networks while effectively circumventing the computational complexity associated with mesh generation and discretization in traditional numerical methods. This approach provides a new paradigm for efficiently solving PDEs and has demonstrated remarkable applicability in various domains, including fluid

[1]School of Mathematics and Statistics, North China University of Water Resources and Electric Power, Zhengzhou 450046, China. [2]School of Water Conservancy, North China University of Water Resources and Electric Power, Zhengzhou 450046, China. [3]School of Mathematics and Statistics, North China University of Water Resources and Electric Power, Zhengzhou 450046, China. ✉email: x202210080830@stu.ncwu.edu.cn; 42125548@qq.com

mechanics[8], solid mechanics[9], and heat conduction[10]. However, existing studies indicate that PINNs still face two major challenges: limitations in generalization performance and numerical stability issues[11,12], particularly when solving problems with strong nonlinearity and complex boundary conditions. Therefore, further optimizing PINNs to address these challenges is crucial for expanding their application to a broader range of complex problems.

In recent years, to enhance the modeling accuracy of PINNs, research has focused on several key areas, including the development of more suitable activation functions[13,14], novel parameter optimization techni*ques*[1516], *im*proved neural network architectures[17–20], and refined loss function structures[21]. These methods have achieved varying degrees of success in specific applications. Additionally, ensemble approaches have demonstrated unique advantages in solving PDEs. For instance, Tartakovsky et al.[22] proposed a physics-informed deep neural network (DNN) approach to estimate hydraulic conductivity in both saturated and unsaturated flows governed by Darcy's law. Experimental results demonstrated that this method can accurately capture the pressure–conductivity relationship in homogeneous porous media, even in the presence of measurement noise. Depina et al.[23] investigated the application of physics-informed neural network to inverse problems in unsaturated groundwater flow. The results indicated that the model is capable of effectively producing reasonably accurate approximations of the model parameters. Haruzi et al.[24] employed non-invasive geoelectrical tools to train a PINN for simulating two-dimensional water flow and solute transport during infiltration and redistribution processes under unknown initial conditions. The results showed that the trained PINN system was able to accurately reproduce the spatiotemporal distribution of water content and pore water salinity in both processes. Alhubail et al.[25] proposed a method that decouples the mass conservation equation and Darcy's law, and trains the PINN using the residuals of these decoupled equations instead of relying on the residual of a single combined equation. This approach not only preserves the inherent discontinuities of petrophysical properties but also leverages the advantages of differential formulations, enabling realistic reservoir simulations to capture subsurface complexities. LIN et al.[26] incorporated diffusion term regularization into the equation and included reference solutions in the loss function as training coefficients, demonstrating that the new algorithm better handles discontinuities without introducing parasitic oscillations. Yan et al.[27] proposed MultiInNet PINNs, which utilize a multi-input residual network combined with a multi-step training paradigm to enhance the stability of PINN training and achieve faster convergence. Inspired by the mixed-form governing equations, Lehmann et al.[28] applied the mass conservation equation and Darcy's law separately within the PINN framework. Numerical experiments demonstrated that each component field with different structural configurations achieved the highest accuracy within an equivalent simulation time, regardless of the type, level, or distribution of heterogeneity. Li et al.[29] integrated the LSTM framework into the solution of PDEs, achieving higher reliability and accuracy while effectively mitigating some of the limitations associated with traditional PINN methods. However, relatively few studies have incorporated flow field measurement data into the PINN training process. *Maziar*[30] and Yang et al.[20] *i*ntroduced flow field measurements to solve both forward and inverse flow problems. Additionally, Maryam et al.[31] applied transfer learning by using low-fidelity computational fluid dynamics (CFD) data to initialize PINNs, significantly improving their modeling accuracy. Liu Xia et al.[32] integrated PINNs with computational fluid dynamics (CFD) simulation results of flow fields, enhancing the modeling accuracy of neural networks. Most PDEs solved using the PINN algorithm in previous studies involve relatively simple nonlinear coefficients. However, the Richards equation presents a significant challenge due to the highly nonlinear relationship between its first- and second-order coefficients and the water content[33], making it considerably more difficult to solve. Huo Haifeng et al.[34] were the first to apply the PINN algorithm to solve the Richards equation. Hydrus is a finite element model designed for simulating one-dimensional movement of water, heat, and multiple solutes in variably saturated media. It incorporates mass conservation equations, momentum conservation equations, and mass transport processes, offering unique advantages in modeling unsaturated soil hydraulics[35–37]. However, its reliance on fixed spatial and temporal discretization grids makes it less adaptable to local feature variations, thereby limiting its applicability in high-resolution simulations.

To overcome the limitations of deep learning methods in handling boundary conditions and data scarcity, as well as the high computational cost and accuracy limitations of traditional finite element (mesh) methods in complex nonlinear problems, this paper proposes a data fusion-based improved PINN algorithm. The proposed method addresses the challenges faced by traditional methods and the classic PINN algorithm in solving the Richards equation, such as high mesh complexity and limited accuracy. By integrating PINN with Hydrus data, the algorithm leverages the strengths of both approaches, resulting in a model that demonstrates higher accuracy and robustness when dealing with complex unsaturated soil infiltration problems. This data fusion approach enables a seamless combination of physical knowledge and data-driven techniques, significantly improving the overall accuracy of infiltration simulations and providing a more efficient and robust solution strategy for unsaturated soil infiltration problems.

Richards equation

The Richards equation is a nonlinear partial differential equation that describes water movement in unsaturated soils. Its core lies in integrating water dynamics with soil physical properties, making it widely applicable in agriculture, environmental engineering, and water resource management. Solving the Richards equation facilitates the optimization of irrigation strategies, assessment of pollutant transport, and prediction of groundwater fluctuations, providing crucial theoretical support and practical guidance for these fields. It enables scientists and engineers to make more informed decisions. The general form of the Richards Equation[38,39] is:

$$\frac{\partial \theta\ (h)}{\partial\, t} = \nabla\ \cdot\ [\mathrm{K(\,h)}\nabla\ (\mathrm{h} + \mathrm{z}\,)] \tag{1}$$

In this study, a one-dimensional vertical water infiltration model is developed for solving the Richards equation. The soil water retention curve is characterized using the Mualem-Van Genuchten (VG) model[40], which describes the relationship between hydraulic conductivity and soil matric potential. Furthermore, the model is applied to solve the highly nonlinear coefficient equations. The governing equation for one-dimensional vertical infiltration is given as follows:

$$\frac{\partial \theta}{\partial t} = \frac{\partial}{\partial z}\left(D(\theta)\frac{\partial \theta}{\partial z}\right) + \frac{\partial K(\theta)}{\partial z} \tag{2}$$

According to the VG model, the equations for calculating $K(\theta)$ and $D(\theta)$ are as follows:

$$K(\theta) = K_s \Theta^{\iota}\left[1-(1-\Theta^{\frac{1}{m}})^{m}\right]^2 \tag{3}$$

$$D(\theta) = K(\theta)\frac{\partial \phi}{\partial \theta} \tag{4}$$

Θ represents the volumetric water content, which is given by

$$\Theta = \frac{\theta - \theta_r}{\theta_s - \theta_r} \tag{5}$$

$$\theta = \theta_r + \frac{\theta_s - \theta_r}{[1+(\alpha\phi)^n]^m} \tag{6}$$

Among them, $\theta(h)$ represents the volumetric water content, which is typically a function of the matric suction head h; z denotes the height in the direction of gravity; and ∇ is the gradient operator. $\nabla = (\frac{\partial}{\partial x}, \frac{\partial}{\partial y}, \frac{\partial}{\partial z})$; $\nabla\cdot$ represents the divergence operator; $\nabla \cdot F = \frac{\partial F_x}{\partial x} + \frac{\partial F_y}{\partial y} + \frac{\partial F_z}{\partial z}$; t represents time; $K(\theta)$ is the unsaturated hydraulic conductivity (m/s); and $D(\theta)$ is the unsaturated diffusivity (m^2/s). K_s represents the saturated hydraulic conductivity; ι is the fitting parameter, set to 0.5; m is an empirical parameter; θ_s denotes the saturated water content; θ_r represents the residual water content; and α、n is an empirical parameter in the VG model.

Algorithm

This section first introduces the classical PINN algorithm and then presents the improved algorithm proposed in this study for solving the Richards equation. The proposed algorithm integrates both data-driven and physics-driven mechanisms, enhancing the model's accuracy and convergence when addressing highly nonlinear problems. The superiority of the improved algorithm over the classical PINN in solving the Richards equation is demonstrated, particularly in handling complex boundary conditions, providing a more efficient and robust approach for unsaturated soil seepage simulation. Additionally, the finite difference method is employed to verify the accuracy of the numerical solutions obtained by PINN.

Classical PINN algorithm

Physics-Informed Neural Network (PINN) integrate neural networks with the physical knowledge of partial differential equations (PDEs) by incorporating the governing equations as constraints within the neural network. This approach enables the model to approximate the solution of PDEs while inherently satisfying physical laws. Typically, a PINN consists of a fully connected neural network with multiple hidden layers and nonlinear activation functions. It establishes a functional relationship between the input (z,t)(where z and t represent temporal and spatial coordinates, respectively) and the output θ. The automatic differentiation technique is then employed to compute the partial derivatives of the network output with respect to the input variables, yielding the residual term $F(z,t)$ of the governing equation. Finally, the residual is used to formulate the loss function, guiding the training process. In the one-dimensional case, the structure of the PINN is illustrated in Fig. 1, and the residual of the equation is defined as follows:

$$F(z,t) = \frac{\partial \theta}{\partial t} - D(\theta)\frac{\partial^2 \theta}{\partial z^2} - \frac{\partial D(\theta)}{\partial z}\frac{\partial \theta}{\partial z} - \frac{\partial K(\theta)}{\partial z} \tag{7}$$

The loss function of the PINN is composed of three components: the equation residual, the initial residual, and the boundary residual. The formulation is given as follows:

$$Loss = w_f Loss_f + w_I Loss_I + w_{Bu} Loss_{Bu} + w_{Bd} Loss_{Bd} \tag{8}$$

The weights corresponding to the loss functions for the governing equation, initial condition, upper boundary condition, and lower boundary condition are denoted as w_f, w_I, w_{Bu}, and w_{Bd}, respectively. The selection of weights is primarily based on prior experience and experimental tuning. By observing the numerical variations of the loss terms during the early stages of training, the issue of one term dominating the training process is avoided. In this case, since the magnitudes of the loss values from different components do not differ significantly, all weight values are set to 1. Similarly, the loss functions associated with the governing equation,

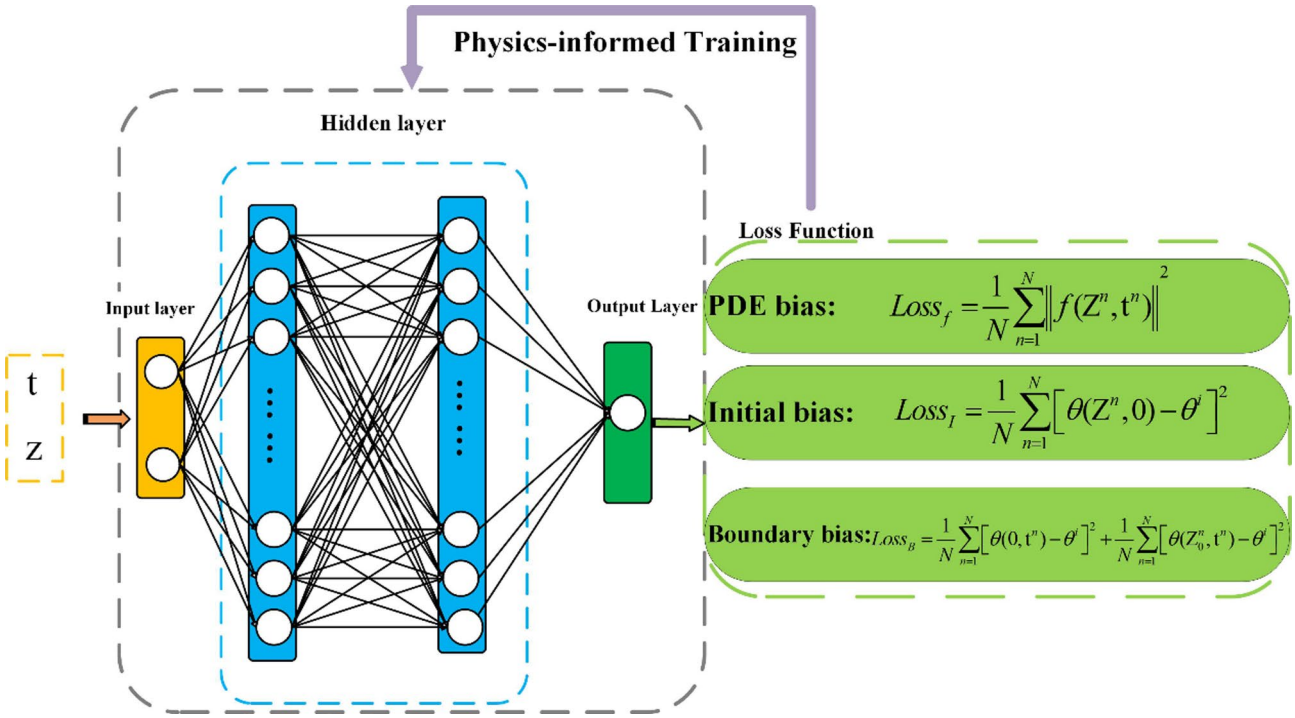

Fig. 1. Diagrammatic sketch of PINN.

initial condition, upper boundary condition, and lower boundary condition are represented by $Loss_f$, $Loss_I$, $Loss_{Bu}$, and $Loss_{Bd}$, respectively. In this study, $Loss_f$, $Loss_I$, $Loss_{Bu}$, and $Loss_{Bd}$ are defined based on the mean squared error (MSE).

$$Loss_f = \frac{1}{N}\sum_{n=1}^{N}\|f(Z^n,t^n)\|^2 \tag{9}$$

$$Loss_I = \frac{1}{N}\sum_{n=1}^{N}[\theta(Z^n,0)-\theta^i]^2 \tag{10}$$

$$Loss_{Bu} = \frac{1}{N}\sum_{n=1}^{N}[\theta(0,t^n)-\theta^i]^2 \tag{11}$$

$$Loss_{Bd} = \frac{1}{N}\sum_{n=1}^{N}[\theta(Z_0^n,t^n)-\theta^i]^2 \tag{12}$$

Here, $\{Z^n,t^n\}_{n=1}^N$ represents the training data, which consists of collocation points randomly selected within the computational domain. The loss function is continuously optimized using either Adam or L-BFGS, allowing the network parameters to be updated iteratively. When the loss function reaches its minimum, the neural network can accurately predict the solution to the equation. Thus, solving the equation is transformed into an optimization problem, where the loss function is minimized through the backpropagation mechanism and optimization algorithms of the neural network. At the beginning of training, if the initial values of different loss functions vary significantly, the weights need to be adjusted to ensure that the magnitudes of all loss terms are comparable; otherwise, the computational efficiency of the network may be reduced. Adam is an adaptive gradient descent method that combines momentum and RMSProp techniques, enabling fast convergence in non-convex problems[41]. It is commonly used for initial training to quickly reach an effective parameter region, significantly improving the convergence speed and stability of neural networks in complex nonlinear problems. Compared to traditional gradient descent methods, Adam performs better when dealing with sparse gradients or non-stationary objective functions, which is why it was selected as the primary optimization strategy in this study.

Hybrid PINN

Through simulation tests, it has been observed that when PINN is solely applied to modeling physical processes described by differential equations, it can result in significant errors, which may accumulate over time. Incorporating computed flow field values or real data can enhance the modeling accuracy of PINN. Therefore, in this study, we propose a data fusion method based on PINN by integrating it with Hydrus simulation results for flow field analysis. Under this fusion framework, the flow field simulation data provided by Hydrus[42] serves as additional supervisory information, which, together with the physical residuals of PINN, constitutes the loss function. This approach effectively reduces the discrepancy between model predictions and the actual physical

process. By leveraging the high-accuracy computational results of Hydrus to guide PINN training, the model achieves improved precision and stability in flow field analysis, offering a novel solution for studying complex nonlinear seepage problems. It is important to note that the simulation data from Hydrus-1D were used to generate synthetic data for training the PINN, and were not integrated into a real-time coupled simulation framework with the PINN model. A schematic diagram of the fusion method is shown in Fig. 2.

At this point, the total loss function of the neural network is given by:

$$Loss = w_f Loss_f + w_I Loss_I + w_{Bu} Loss_{Bu} + w_{Bd} Loss_{Bd} + w_D Loss_D \tag{13}$$

Where:

$$Loss_f = \frac{1}{N} \sum_{n=1}^{N} \| f(Z^n, t^n) \|^2 \tag{14}$$

$$Loss_I = \frac{1}{N} \sum_{n=1}^{N} [\theta\,(Z^n, 0) - \theta^i]^2 \tag{15}$$

$$Loss_{Bu} = \frac{1}{N} \sum_{n=1}^{N} [\theta\,(0, t^n) - \theta^i]^2 \tag{16}$$

$$Loss_{Bd} = \frac{1}{N} \sum_{n=1}^{N} [\theta\,(Z_0^n, t^n) - \theta^i]^2 \tag{17}$$

$$Loss_D = \frac{1}{N_D} \sum_{n=1}^{N_D} [\theta_{Hydrus}(Z^n, t^n - \theta^i)]^2 \tag{18}$$

Where w_f, w_I, w_{Bu}, w_{Bd}, and w_D are the weights corresponding to the loss functions of the governing equation, initial condition, upper boundary condition, lower boundary condition, and the Hydrus-1D data component, respectively. Similarly, $Loss_f$, $Loss_I$, $Loss_{Bu}$, $Loss_{Bd}$, and $Loss_D$ represent the loss functions associated with the governing equation, initial condition, upper boundary condition, lower boundary condition, and the Hydrus-1D data component, respectively. The variable $\theta_{Hydrus}(Z, t)$ denotes the flow field data exported from Hydrus-1D. N_D represents the total dataset collected from Hydrus-1D. Table 1 provides

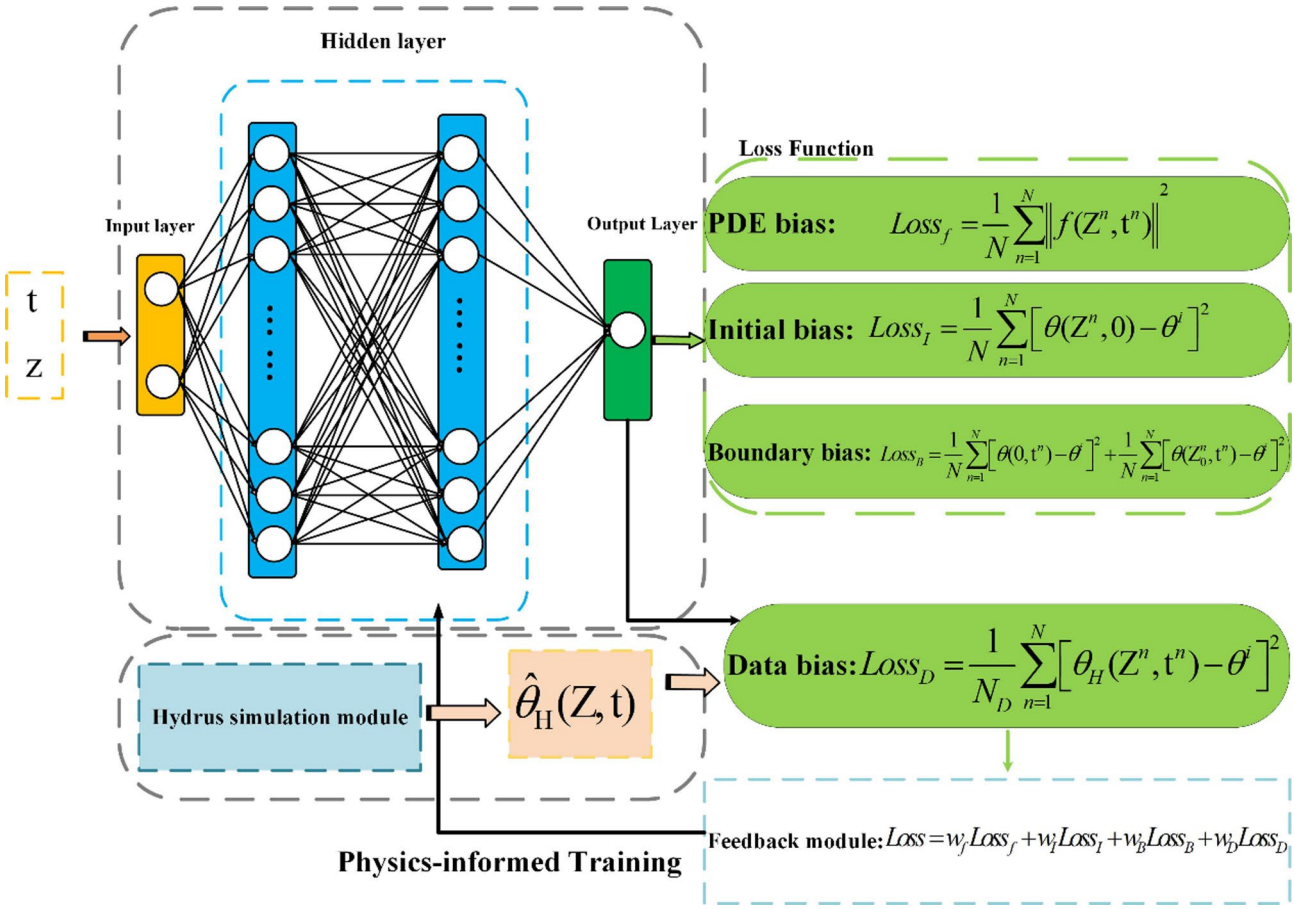

Fig. 2. Hybrid PINN.

Category	Symbol	Meaning	Type	Classical PINN	Hybrid PINN
State Variable	$\theta\ (z,t)$	Water Content	Model output	Objective Function of the Network Prediction	
Input Variable	z/t	Depth/Time	Model Input	Range [0, Z]/Range [0, t]	
	$\theta\ (z,0)$	Initial Water Content		Residual of Initial Conditions Incorporated into the Loss Function	
	$\theta\ (0,t)$ $\theta\ (z_0,t)$	Upper and Lower Boundary Conditions		Residual of Boundary Conditions Incorporated into the Loss Function	
Hydrus-1D Data	$\theta_{data}(z,t)$	Water Content Field	Data-Driven Input	Not Incorporated	Incorporation
Soil Parameters	θ_s/θ_r	Saturated/Residual Water Content	Calibrated Parameters	See Table 2	
	K_s	Saturated Hydraulic Conductivity			
	$\alpha\ /m/n$	VG Model Parameters			

Table 1. Comparison of variables and parameters between the two PINN models. In this study, two PINN frameworks are considered:. (1) Classic PINN: This framework fully relies on physical equations without any measurement data;.

a systematic summary of the proposed PINN model, including its inputs, outputs (state variables), involved physical parameters, and calibration methods, aiming to offer a clearer understanding of the model construction and solution process.

(2) Improved PINN: Also referred to as Hybrid PINN, this approach integrates a small portion of measurement data or flow field data (e.g., Hydrus-1D) into the loss function to enhance the model's generalization capability and avoid data waste in practical applications.

The Hybrid PINN in this paper refers to the data fusion PINN model, defined by the modified loss function in Eq. (18). This study focuses on several limitations of the classic PINN in groundwater infiltration processes, such as low accuracy and unstable training. To address these issues, we propose an improved PINN model that incorporates a small amount of data generated by Hydrus-1D (referred to as Hybrid PINN). By introducing a data-driven term, the model's solvability and stability are improved, resulting in more generalized predictions under real-world conditions. From this point onward, we will primarily use the term Hybrid PINN.

Numerical example

In this study, the neural network framework is implemented using Python. When solving the Richards equation, the temporal and spatial domains of the target model are first defined. The governing equation is embedded into the neural network through automatic differentiation, and the input and output variables are specified accordingly. Boundary residual points are selected and assigned values, ensuring that all well-posed conditions are incorporated into the neural network. A feedforward neural network (FNN) was constructed with an input layer comprising two neurons, corresponding to the two independent variables in the equation: depth and time. The output layer consists of a single neuron. The hyperbolic tangent (Tanh) function, which is infinitely differentiable, was selected as the activation function. Based on extensive experimentation and prior studies, this work found that configuring the network with six hidden layers, each containing 32 neurons, achieves a favorable balance among training stability, fitting accuracy, and computational efficiency[34]. To enhance the generalization performance of the model, simulations are conducted using three different media: unsaturated soft clay (S1), sandy loam unsaturated silt (S2), and unsaturated silt (S3). The model is applied to simulate one-dimensional infiltration in unsaturated soil under surface ponding conditions, with parameters consistent with those of the respective media. The total height of the soil model is 1 m, with an initial moisture content of 0.1. The upper surface of the soil is continuously supplied with water, maintaining a constant moisture content that is close to saturation, while the lower boundary is set as a free drainage condition. The corresponding initial conditions for the equation are as follows:

$$\theta\ (z,0) = 0.10 \tag{19}$$

The boundary conditions for S1 and S3 are $\theta\ (0,t) = 0.45$, while the boundary condition for S2 is $(0,t) = 0.40$.

By initializing the residual points, the training and testing datasets are selected as input variables for the network within the computational domain. The number of residual points in the computational domain for the training set is initialized to 10,201, with 101 residual points initialized on the spatial boundaries and 101 residual points initialized on the time boundaries. The training points are uniformly selected. During the training process, the Adam gradient descent algorithm is used to update the network parameters. After several adjustments to the computational step size, it was found that setting the step size to 10,000 steps allowed both the training and testing errors of the neural network to decrease to a stable value, and the final error met the required specifications.

The relevant physical parameters of the soil types are shown in Table 2.

Taking unsaturated soft clay (S1) as an example, after 10,000 iterations, the 3D and 2D plots of the classical PINN numerical solution for the constant coefficient one-dimensional infiltration equation are shown in Fig. 3. The 3D and 2D plots of the PINN numerical solution are shown in Fig. 4.

Soil types	Soft clay(s1)	Sandy loam(s2)	Silty soil(s3)
Physical parameters	Numerical value	Numerical value	Numerical value
θ_s	0.46	0.41	0.46
θ_r	0.02	0.065	0.34
$K_s/(m \cdot h^{-1})$	0.036	0.044	0.0025
α	0.29	7.5	1.6
n	1.33	1.89	1.37
m	0.248	0.47	0.27

Table 2. Physical parameters of soil types. K_s(unit: m/h) represents the ability of water to flow through saturated soil. α is a fitting parameter ($1/m$) that controls the steepness of the soil water retention curve. n and m are empirical parameters in the VG model that describe the pore size distribution. θ_r and θ_s are dimensionless, with values ranging from 0 to 1.

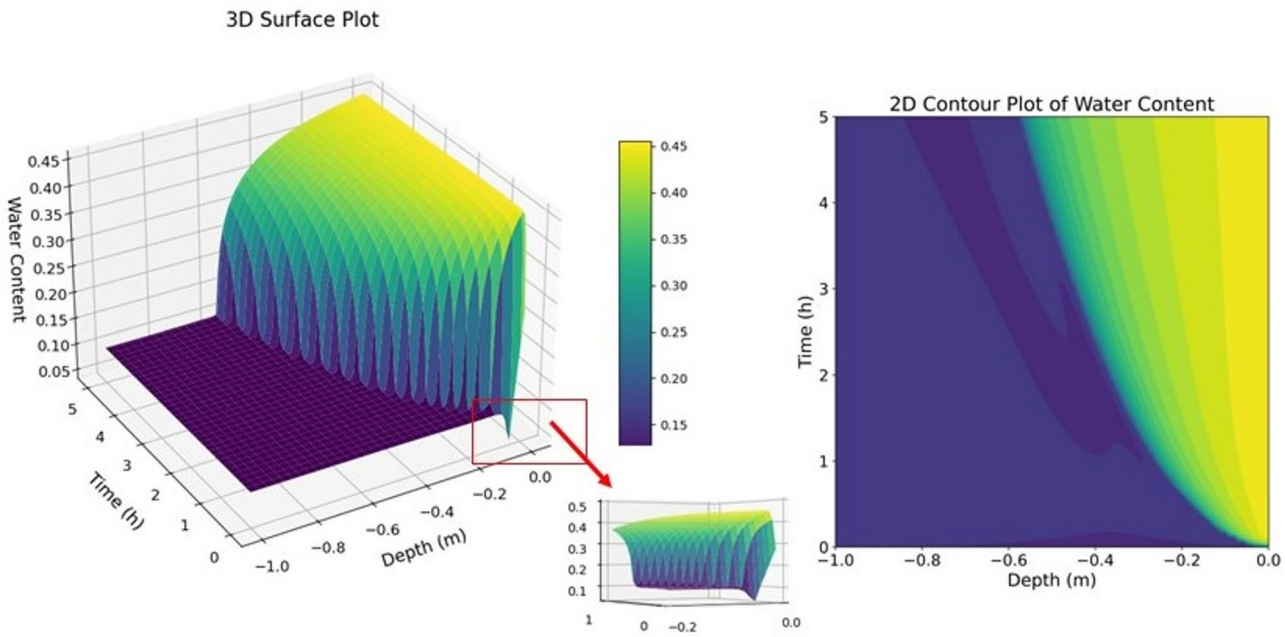

Fig. 3. Classic PINN Prediction Diagram.

From Figs. 3 and 4, it can be observed that both the classical PINN and the Hybrid PINN exhibit overall trends in moisture content variation with depth and time that align with the basic physical characteristics of the Richards equation, indicating that they can be used for modeling unsaturated soil infiltration processes. However, in the 3D surface plot of Fig. 3, significant oscillations are present, particularly in areas close to the boundary (near depth 0), where the surface displays noticeable sawtooth-like fluctuations. In contrast, the 3D plot in Fig. 4 shows a much smoother transition near the boundary, without abrupt changes or unreasonable fluctuations. This suggests that the classical PINN may exhibit instability and accuracy degradation in scenarios with scarce data or complex boundary conditions. The Hybrid PINN demonstrates more stable and accurate performance in modeling unsaturated soil infiltration problems and better adheres to physical laws.

To visually highlight the performance differences between the classical PINN and the Hybrid PINN algorithms, moisture content distribution curves at different depths at the same time and at the same depth over different times are selected for the soils under scenarios S1, S2, and S3. In the S1 and S2 scenarios, due to the relatively fast water movement in the soil and the practical application needs (such as agricultural irrigation and urban drainage design), which typically focus on moisture changes over a short period of time, 5 h is chosen. However, in the S3 scenario, the high clay content, low permeability, and complex pore structure of the silt soil cause slower moisture movement and less pronounced changes in the soil. Therefore, to observe significant effects in the simulation of moisture content change in silt soil, a longer duration (such as 192 h) is required. Since the depth range from 0.1 to 0.3 m corresponds to the topsoil, which is sensitive to environmental and plant root activities, it satisfies the practical needs of agricultural irrigation and ecological environment studies. Therefore, in all three scenarios, the depth is chosen to range from 0.1 to 0.3 m.

By comparing the prediction results from the finite difference method, which serves as the reference solution, with the results from the PINN simulation, the accuracy and trend differences at various time points are analyzed

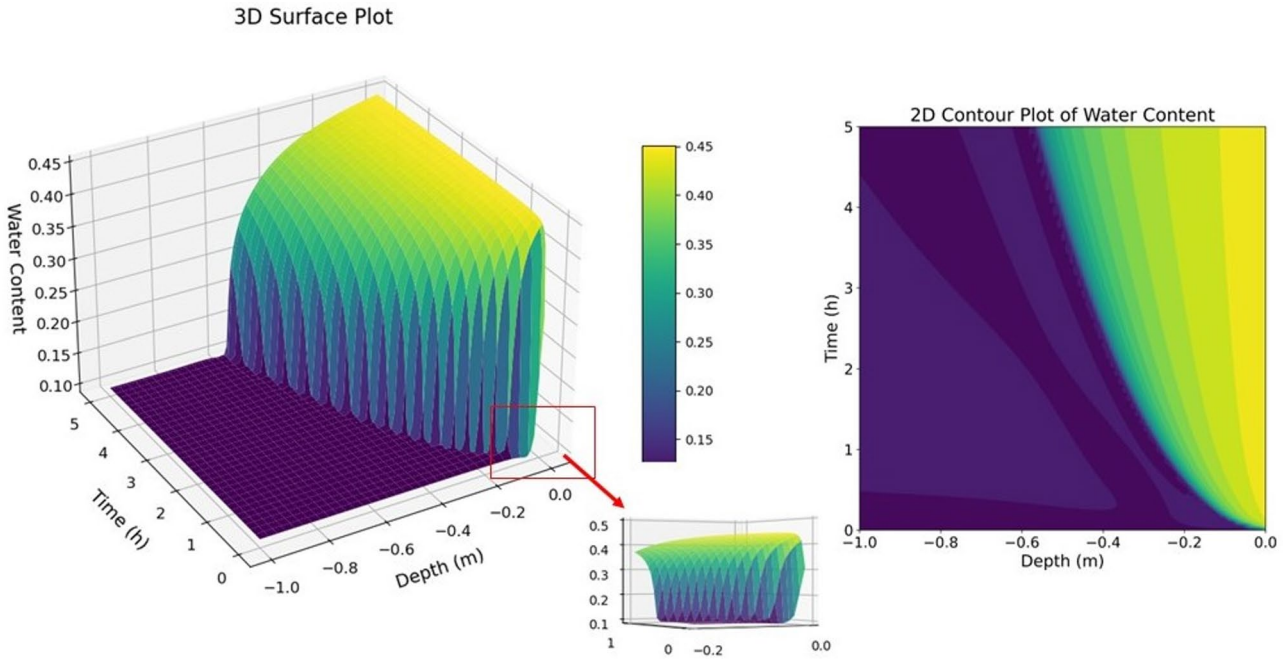

Fig. 4. Hybrid PINN Prediction Diagram.

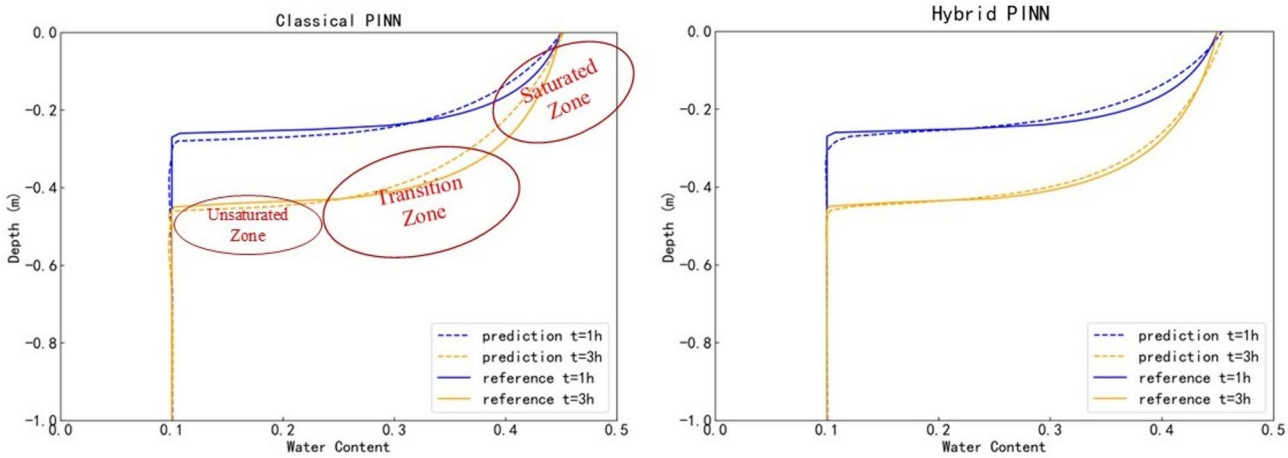

Fig. 5. Moisture content variation with depth in soft clay.

to further validate the superiority of the Hybrid PINN algorithm in simulating the moisture variation process in unsaturated soils. It is important to note that although the finite difference simulation and the PINN model employ the same soil physical parameters (e.g., θ_r; θ_s; m; n; α), the simulation results were not involved in the training process of the PINN, nor were any observational data or boundary conditions shared between them. Therefore, the validation remains relatively independent and can effectively reflect the generalization capability of the model. The comparison plots for the s1 s1 s1 scenario are shown in Figs. 5 and 6.

From Fig. 5, it can be observed that the PINN predictions align with the reference numerical solution, and the predicted moisture content at different depths closely matches the reference values. However, in the classical PINN numerical solution, small errors appear in the unsaturated zone (moisture content between 0.1 and 0.2), and in the transition zone (moisture content between 0.2 and 0.4), the curve deviates significantly from the reference curve, showing considerable fluctuations. In the saturated zone (moisture content between 0.4 and 0.5), larger errors are observed in some localized areas. In contrast, the Hybrid PINN demonstrates higher accuracy and stability across different moisture ranges, enhancing the reliability of the numerical solution and making the simulation results better reflect the actual physical process. Therefore, it can be concluded that the Hybrid PINN provides a certain level of accuracy in predicting the moisture distribution at different times during the surface water infiltration process. Next, the moisture content variation with time at depths of 0.2 m and 0.3 m is further extracted, as shown in Fig. 6.

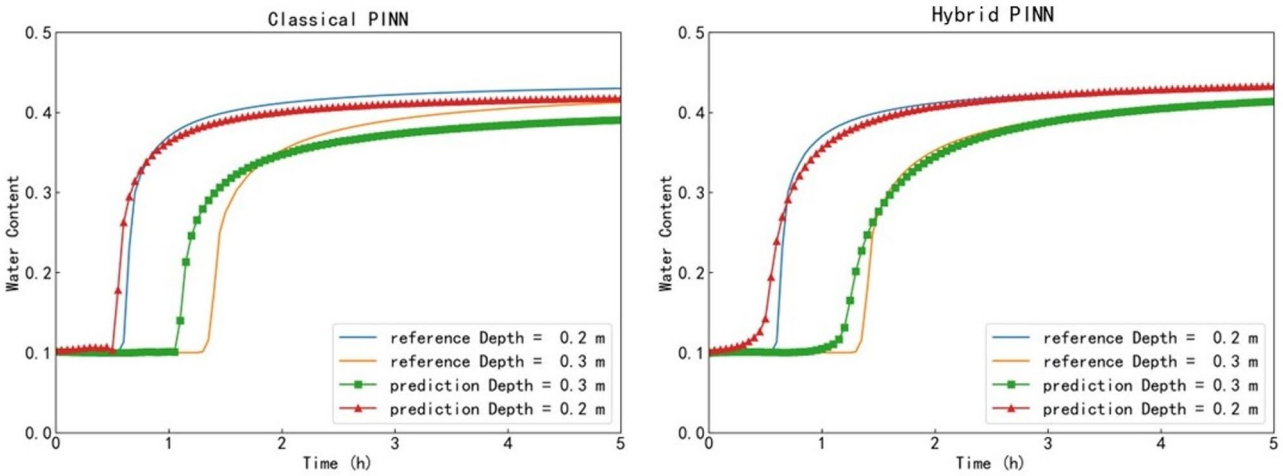

Fig. 6. Moisture content variation with time in soft clay.

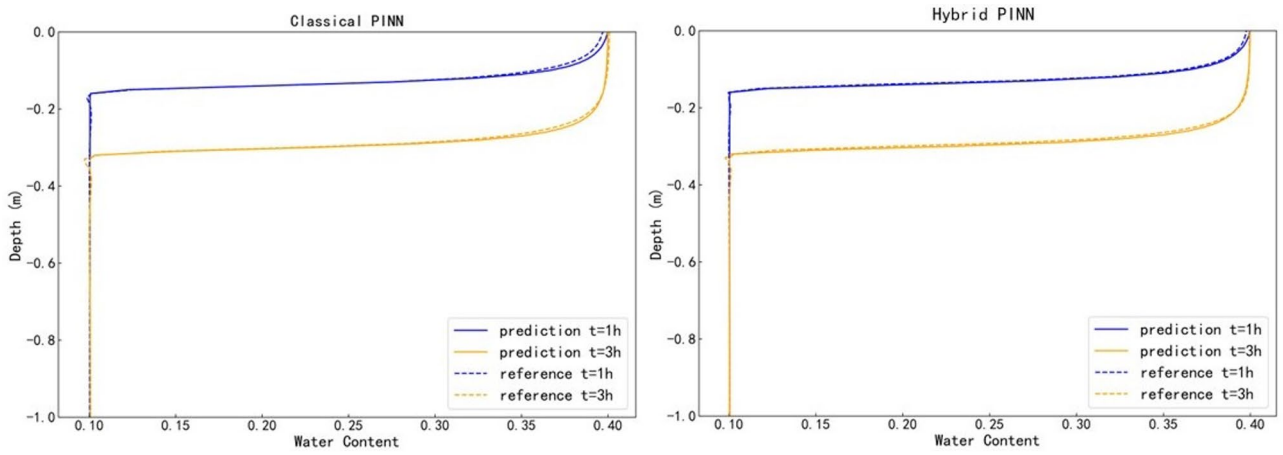

Fig. 7. Moisture content variation with depth in sandy loam.

From Fig. 6, it can be observed that the moisture content at depths of 0.2 m and 0.3 m gradually approaches the surface moisture content over time, with the final stable value being less than 0.45. However, at depths of 0.2 m and 0.3 m, the classic PINN prediction curves exhibit a lag, failing to capture the precise dynamics of moisture change. In contrast, the Hybrid PINN prediction curves are clearly closer to the reference solution, indicating that as the simulation time increases, the Hybrid PINN model provides higher accuracy than the classical PINN model, offering more precise and faster predictions of moisture content.

The comparison results in the s2 scenario are shown in Figs. 7 and 8.

From Fig. 7, it can be observed that in sandy loam, the classic PINN exhibits significant oscillations at a moisture content of 0.1, with fewer errors in the saturated zone, while the Hybrid PINN is closer to the reference solution. From Fig. 8, it can be seen that the classic PINN shows errors at the corners of the unsaturated zone and exhibits some deviation from the reference solution in the transition zone, whereas the Hybrid PINN is overall closer to the reference solution and is smoother at the corners of the unsaturated zone.

The comparison results in the s3 scenario are shown in Figs. 9 and 10.

Overall, the Hybrid PINN demonstrates superior simulation performance over the classic PINN across multiple time points and depth conditions, especially excelling in long-term moisture distribution prediction. In practical engineering, by simply obtaining parameters such as the saturated moisture content, residual moisture content, and saturated permeability coefficient, the corresponding unsaturated soil infiltration model can be trained using the PINN algorithm to predict the moisture content of the soil at different times and locations during the infiltration process.

In the three different media, the Hybrid PINN shows that the moisture content curves are much closer to the reference solution. By quantifying the overall error with the Root Mean Square Error (RMSE), it becomes evident that smaller RMSE values indicate better numerical simulation performance. The RMSE values, shown in Table 3, clearly demonstrate that the data fusion-based PINN algorithm has smaller overall errors compared to the classic PINN. Moreover, from the comparison plots, it is observable that the Hybrid PINN is more closely

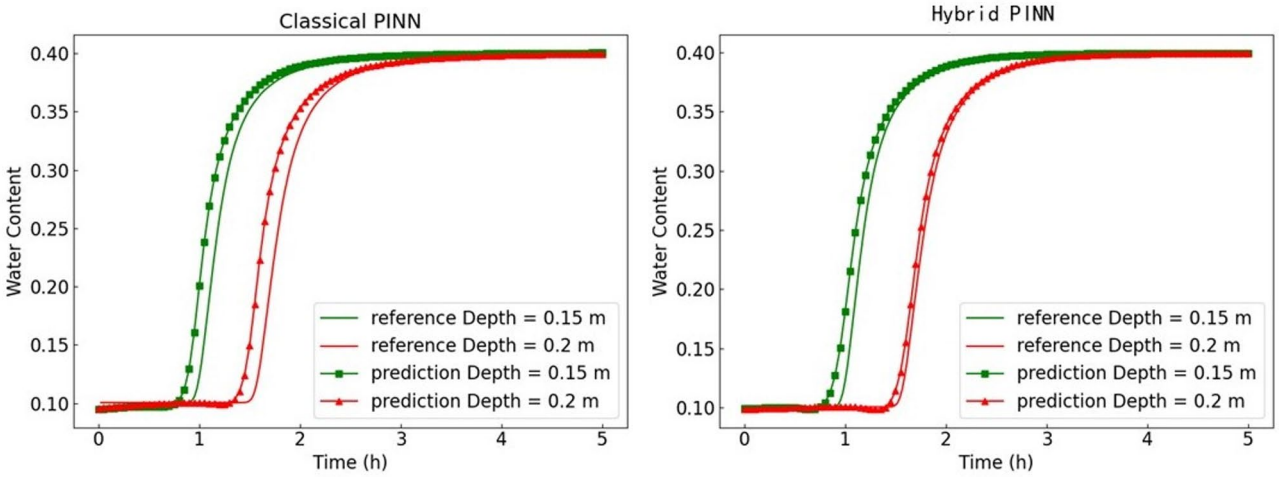

Fig. 8. Moisture content variation with time in sandy loam.

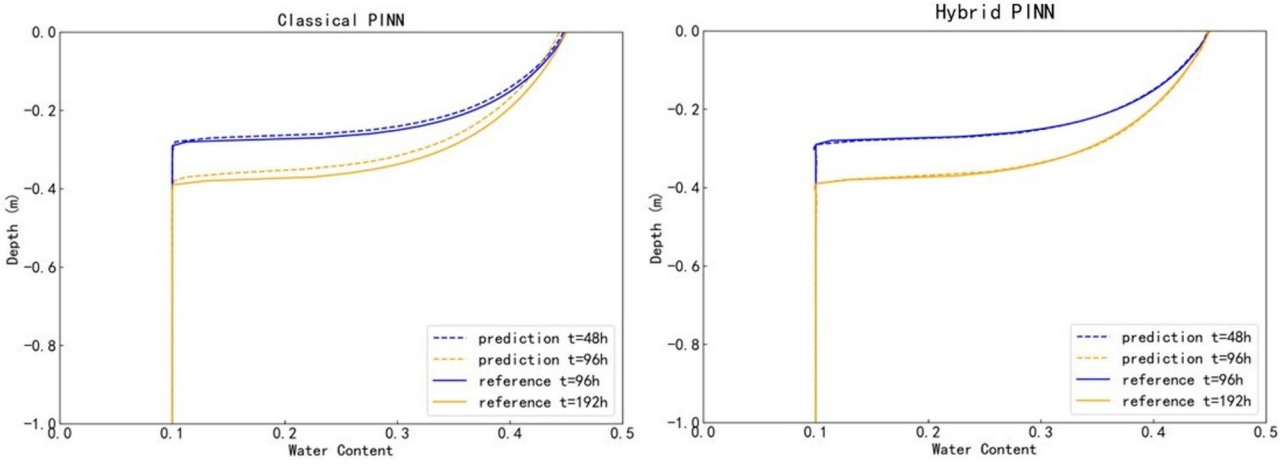

Fig. 9. Moisture content variation with depth in silty soil.

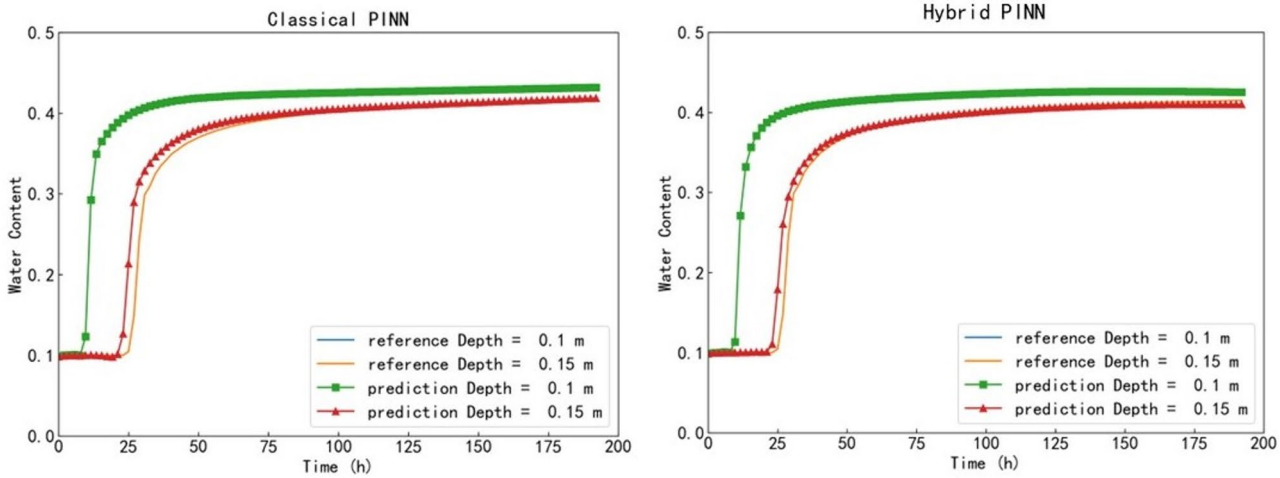

Fig. 10. Moisture content variation with time in silty soil.

Soil type	S1	S2	S3
Classical PINN	0.023	0.026	0.024
Hybrid PINN	0.016	0.017	0.015

Table 3. RMSE values for three soil types.

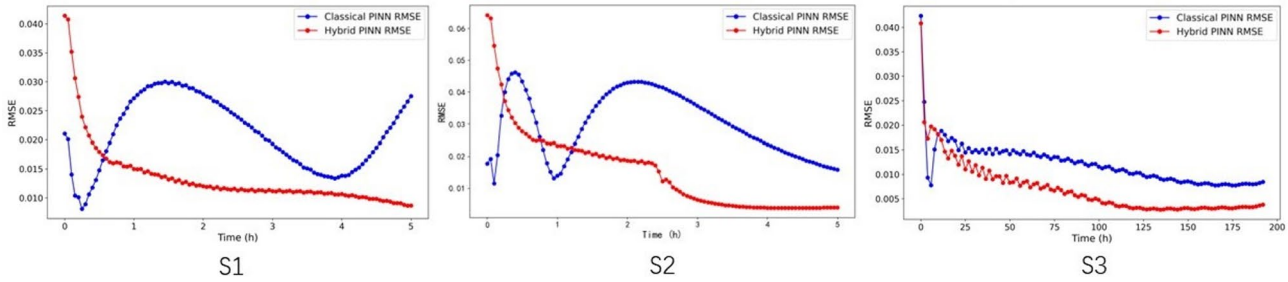

Fig. 11. RMSE Variation Curve with Time.

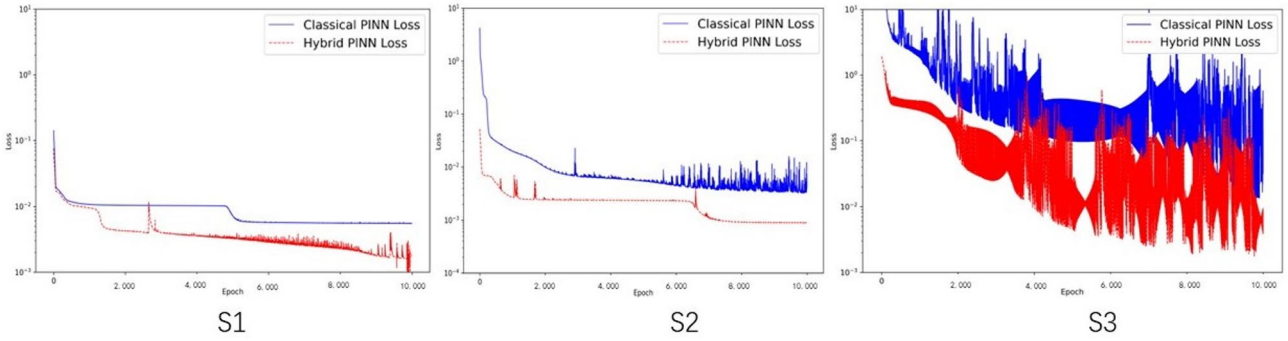

Fig. 12. Comparison of Loss Functions.

aligned with the reference solution. Therefore, the Hybrid PINN provides more stable numerical solutions and higher accuracy in describing the system's true dynamic behavior.

As can be seen from Fig. 11 the RMSE values of the Hybrid PINN method are significantly lower than those of the original method. Particularly over longer time periods, the RMSE of the improved method remains within a lower range, indicating that the Hybrid PINN method provides more accurate predictions for the model. Additionally, it can be observed that over time, the Hybrid PINN method exhibits better steady-state performance, with the RMSE gradually stabilizing and remaining at a low level. This demonstrates the stability and accuracy of the improved method in long-term predictions.

Figure 12 below shows a comparison of the loss function convergence during the training process between PINN and the Hybrid PINN. By comparing the trend of the loss function over training epochs, we can intuitively observe that during the first few hundred iterations, the loss value decreases rapidly, indicating that the model starts to learn quickly. Moreover, the loss value of the fusion PINN algorithm remains relatively low and fluctuates within a small range. The results show that although the improved algorithm also experiences some fluctuations in the loss value, the overall amplitude of these fluctuations is smaller, indicating that the improved algorithm exhibits better stability during training. Additionally, the PINN method outperforms the classical method in both the convergence speed and the final value of the loss function. The results of the PINN algorithm integrated with Hydrus-1D data align more closely with the actual observations.

Discuss

In this study, we innovatively propose a data-fusion approach based on Physics-Informed Neural Networks (PINN) to capture the dynamic moisture variations in unsaturated soil infiltration processes. As a cutting-edge technique for data processing and modeling, PINN exhibits unique advantages in handling data related to complex physical processes. By integrating PINN with Hydrus data, we leverage the strengths of both methodologies. Although both approaches are derived from the Richards equation, they adopt fundamentally different solution strategies. Essentially, PINN is a deep neural network architecture that inherently incorporates the trend information of differential equations when processing data. In contrast, Hydrus-1D simulations rely on domain experts who embed substantial professional knowledge and experience during mesh generation.

This process captures detailed flow field information, such as localized moisture variations under different soil textures and pore structures. The study employs both the classical PINN and the Hybrid PINN algorithms for simulation and comparison. Experimental results across multiple scenarios (S1, S2, S3) demonstrate that the Hybrid PINN exhibits higher accuracy and stability compared to the classical PINN. It more effectively captures moisture dynamics while mitigating oscillations and instabilities caused by data scarcity or complex boundary conditions. Furthermore, RMSE comparisons provide additional evidence that the improved algorithm significantly enhances prediction accuracy and reliability, particularly for long-term simulations. In terms of computational efficiency, the proposed hybrid PINN model adopts the same network architecture as the classical PINN model. Therefore, under identical hardware conditions, their runtimes are comparable. On an NVIDIA GeForce RTX 4060 GPU, the classical PINN model required 162.3 s to complete 10,000 iterations, while the hybrid PINN model took 166.4 s. These results indicate that although data-driven components were introduced, the additional computational cost was negligible. The model maintains high accuracy and stability while still offering good computational efficiency and scalability.

When integrating PINN with Hydrus-1D data, the complementary strengths of both approaches enhance the accuracy of infiltration data fusion. Case studies involving three different soil types clearly demonstrate that incorporating Hydrus-1D data significantly improves the modeling accuracy of PINN.A noteworthy observation is that the magnitude of the loss function does not necessarily reflect the quality of PINN's fitting performance. For instance, in scenario S3, the PINN loss function is larger than in S1 and S2, yet the overall relative error is smaller. This phenomenon highlights the limitation of relying solely on PINN or focusing exclusively on the fitting accuracy of partial differential equations. It further underscores the necessity of the proposed fusion method, which overcomes the constraints of a single approach by effectively extracting and utilizing valuable information from diverse data sources. Therefore, during practical training, convergence of the loss function should not be used as the sole criterion. It is advisable to incorporate validation error as a complementary metric for comprehensive evaluation. Furthermore, introducing periodic monitoring indicators based on physical consistency or predictive accuracy in the later stages of training can enhance model stability. This phenomenon also offers new insights into the development of adaptive sampling methods, loss reweighting strategies for handling strongly nonlinear boundary conditions, and dynamic training schemes.

In practical hydrological modeling and groundwater management, the data required for model training is not necessarily limited to numerical solutions generated by software such as Hydrus. It can also be flexibly integrated with field monitoring data, remote sensing data, or results from other simulations for training and validation. This flexibility enables the PINN model to retain practical value in scenarios where complete physical parameters are unavailable or complex solvers cannot be constructed. Moreover, the "train-then-predict" nature of PINNs supports online prediction applications. Once trained with existing data, the model can be used for real-time forecasting or for simulating hydrodynamic behavior under varying boundary conditions, making it particularly suitable for embedded systems or data-driven monitoring platforms. Although this approach may involve a high computational cost during the training phase, it offers significant advantages in the prediction phase, including high computational efficiency and fast response time. This provides a novel perspective for addressing real-world engineering problems such as groundwater management, irrigation scheduling, and risk assessment. Meanwhile, following the introduction of a data fusion strategy, our next research objective is to explore how to more effectively integrate data from diverse sources for real-time updates, and to further investigate the model's predictive capability beyond the spatiotemporal range of the training domain.

The PINN method proposed in this study, which integrates physical knowledge and data fusion, demonstrates practical applicability. Compared with traditional numerical methods, this model offers several advantages: (1) when sufficient field observation data are available, data-driven mechanisms can enhance solution accuracy and model robustness; (2) it is applicable to complex scenarios where soil parameters or boundary conditions cannot be accurately obtained. However, certain challenges may arise during practical deployment, such as: (1) model parameters, including weight selection and neural network architecture, are relatively sensitive and require tuning according to specific scenarios; (2) under multidimensional complex terrains or strongly heterogeneous conditions, further exploration of network structure improvements is necessary to enhance generalization performance and mass conservation. Nevertheless, the findings of this study provide a theoretical foundation and technical support for subsequent applications in real-world unsaturated flow scenarios and demonstrate promising potential for broader adoption.

Conclusion

This study is the first to integrate Hydrus-1D software with the PINN algorithm for data fusion, solving the highly nonlinear Richards infiltration model and obtaining high-accuracy numerical solutions. This approach provides a novel solution framework for predicting soil moisture distribution under external water supply conditions. Compared to traditional neural networks, it significantly enhances the model's solution accuracy. The data-fusion-based PINN algorithm offers the following advantages:

(1) The Hybrid PINN constrains the numerical model using physical equations while integrating more accurate data. Compared to the classical PINN, it significantly enhances the solution accuracy and maintains clear physical interpretability.
(2) The Hybrid PINN can accurately solve partial differential equations under different boundary conditions, whereas the classical PINN exhibits poor generalization capability across problems with varying prescribed conditions. Although consistent initial conditions were used across all numerical experiments in this study, the proposed method itself possesses good generality and, in theory, can be applied to a wide range of initial and boundary condition combinations.

(3) Traditional neural networks heavily rely on large amounts of labeled data during training. In contrast, the data-fusion-based Hybrid PINN method proposed in this study combines physical knowledge with a small number of observational data, achieving high prediction accuracy even under data-scarce conditions. Compared with traditional neural network models, this method demonstrates stronger robustness and adaptability in small-sample scenarios.

Data availability

Data is provided within the manuscript.

Received: 10 March 2025; Accepted: 16 May 2025
Published online: 28 May 2025

References

1. Zeng, J., Cha, Y. & Yang, J. Numerical simulation of soil water flow and solute transport based on the switching Richards equation. *J. Hydraul. Eng.* **49**, 840–848. https://doi.org/10.13243/j.cnki.slxb.20180288 (2018).
2. Zhou, W. & Wei, X. Study on numerical solution methods for the Richards equation. *J. Irrig. Drain.* **34**, 277–280. https://doi.org/10.13522/j.cnki.ggps.2015.z1.067 (2015).
3. Cao, L. Deep learning applications. *IEEE. Intell. Syst.* **37**, 3–5. https://doi.org/10.1109/mis.2022.3184260 (2022).
4. Liu, X., Min, J., Yu, X. & Guo, Y. Application and research progress of physics-informed neural networks. *Henan Sci.* **42**, 945–959 (2024).
5. Jayashree, P. & Dibakar, C. Infilling of missing data in groundwater pollution prediction models using statistical methods. *Hydrol. Sci. J.* https://doi.org/10.1080/02626667.2023.2258867 (2023).
6. Xiazi, Y., Balati, M., Zibibula, S., Muattar, S. & Na, L. Prediction of glacially derived runoff in the muzati river watershed based on the PSO-LSTM model. *Water* https://doi.org/10.3390/w14132018 (2022).
7. Raissi, M., Perdikaris, P. & Karniadakis, G. E. Physics-informed neural networks: A deep learning framework for solving forward and inverse problems involving nonlinear partial differential equations. *J. Comput. Phys.* **378**, 686–707 (2019).
8. Tian, S., Huang, X., Duan, Y., Chen, H. & Chen, W. Review of physics-informed neural networks for fluid mechanics. *J. Comput. Appl.* **44**, 133–141 (2024).
9. Chengping, R., Hao, S. & Yang, L. Physics-Informed deep learning for computational elastodynamics without labeled data. *J. Eng. Mechanics-asce*. https://doi.org/10.1061/(asce)em.1943-7889.0001947 (2021).
10. Chen, H., Tang, X., Wang, R., Zhou, H. & Liu, Z. Study on multi-medium nonlinear transient heat conduction based on physics-informed neural networks. *Chinese J. Theoretical Appl. Mechanics*, 1–13
11. Cha, W., Li, D., Shen, L., Zhang, W. & Liu, X. Review of neural network-based methods for solving partial differential equations. *Chin. J. Theoretical Appl. Mech.* **54**, 543–556 (2022).
12. Li, Y. & Chen, S. Physics-informed neural networks: recent advances and future prospects. *Comput. Sci.* **49**, 254–262 (2022).
13. Ameya, D. J. & Kenji, K. George Em, K. Adaptive activation functions accelerate convergence in deep and physics-informed neural networks. *J. Comput. Phys.* https://doi.org/10.1016/j.jcp.2019.109136 (2020).
14. Cheng, C. & Guangtao, Z. Deep learning method based on physics informed neural network with resnet block for solving fluid flow problems. *Water* (2021). https://doi.org/10.3390/w13040423
15. Qi, H., David, A. B. S., Tartakovsky, G. & Alexandre, M. T. Physics-informed neural networks for multiphysics data assimilation with application to subsurface transport. *Adv. Water Resour.* https://doi.org/10.1016/j.advwatres.2020.103610 (2020).
16. Yinhao, Z., Nicholas, Z., Phaedon-Stelios, K. & Paris, P. Physics-constrained deep learning for high-dimensional surrogate modeling and uncertainty quantification without labeled data. *J. Comput. Phys.* https://doi.org/10.1016/j.jcp.2019.05.024 (2019).
17. Ameya, D. J., Ehsan, K. & George Em, K. Conservative physics-informed neural networks on discrete domains for conservation laws: Applications to forward and inverse problems. *Comput. Methods Appl. Mech. Eng.* https://doi.org/10.1016/j.cma.2020.113028 (2020).
18. Ehsan, K., Zhongqiang, Z. & George Em, K. hp-VPINNs: variational physics-informed neural networks with domain decomposition. *Comput. Methods Appl. Mech. Eng.* https://doi.org/10.1016/j.cma.2020.113547 (2021).
19. Han, G., Luning, S., Jianxun, W. & PhyGeoNet Physics-informed geometry-adaptive convolutional neural networks for solving parameterized steady-state PDEs on irregular domain. *J. Comput. Phys.* https://doi.org/10.1016/j.jcp.2020.110079 (2021).
20. Yang, L., Xuhui, M. & George Em, K. B-PINNs: bayesian physics-informed neural networks for forward and inverse PDE problems with noisy data. *J. Comput. Phys.* https://doi.org/10.1016/j.jcp.2020.109913 (2021).
21. Zixue, X., Wei, P., Xiaohu, Z., Guannan, W. & Wen, Y. Self-adaptive loss balanced Physics-informed neural networks for the incompressible Navier-Stokes equations. *arXiv (Cornell University)* https://doi.org/null (2021).
22. Alexandre, M. T., Carlos Ortiz, M., Paris, P., Tartakovsky, G. & David, A. B. S. Physics-Informed deep neural networks for learning parameters and constitutive relationships in subsurface flow problems. *Water Resour. Res.* https://doi.org/10.1029/2019wr026731 (2020).
23. Ivan, D., Saket, J., Sigurdur Mar, V. & Hrvoje, G. Application of physics-informed neural networks to inverse problems in unsaturated groundwater flow. *Georisk: Assess. Manage. Risk Eng. Syst. Geohazards*. https://doi.org/10.1080/17499518.2021.1971251 (2021).
24. Peleg, H. & Ziv, M. Modeling water flow and solute transport in unsaturated soils using Physics-Informed neural networks trained with geoelectrical data. *Water Resour. Res.* https://doi.org/10.1029/2023wr034538 (2023).
25. Ali, A., Marwan, F., François, L. & Hussein, H. Physics-Informed neural networks for modeling flow in heterogeneous porous media: A decoupled Pressure-Velocity approach. *Null* https://doi.org/10.2523/iptc-24362-m (2024).
26. Yunyun, L., Zheng, S., Feng, J. & Fang, J. Diffusive regularization inverse PINN solutions to discontinuous problems. *Yingyong Shuxue He Lixue*. **44**, 112–122. https://doi.org/10.21656/1000-0887.430010 (2023).
27. Liangliang, Y., You, Z., Liu, H. & Laijun, L. An improved method for Physics-Informed neural networks that accelerates convergence. *IEEE Access*. https://doi.org/10.1109/access.2024.3354058 (2024).
28. François, L., Marwan, F., Ali, A. & Hussein, H. A mixed pressure-velocity formulation to model flow in heterogeneous porous media with physics-informed neural networks. *Adv. Water Resour.* https://doi.org/10.1016/j.advwatres.2023.104564 (2023).
29. Li, Y., Sun, Q., Wei, J. & Huang, C. An improved PINN algorithm for shallow water equations driven by deep learning. *Symmetry* **16**, 1376–1376 (2024).
30. Maziar, R., Paris, P. & George, K. Physics-informed neural networks: A deep learning framework for solving forward and inverse problems involving nonlinear partial differential equations. *J. Comput. Phys.* https://doi.org/10.1016/j.jcp.2018.10.045 (2019).
31. Maryam, A., Mahmoudi, M., Péter, V. & Amirhossein, A. Predicting high-fidelity multiphysics data from low-fidelity fluid flow and transport solvers using physics-informed neural networks. *Int. J. Heat Fluid Flow*. https://doi.org/10.1016/j.ijheatfluidflow.2022.109002 (2022).

32. Liu, X. et al. Physics-informed neural network-based aerodynamic data fusion method. *Acta Aerodynamica Sinica*. **41**, 87–96 (2023).
33. Michal, K., Petr, M. & Pavel, P. Solving the nonlinear Richards equation model with adaptive domain decomposition. *J. Comput. Appl. Math.* https://doi.org/10.1016/j.cam.2014.03.010 (2014).
34. Huo, H., Huang, H., Li, Q., Hu, B. & Zhang, Z. Study of highly nonlinear Richards infiltration model based on PINNs. *J. Civil Aviat. Wniversity China*. **41**, 6–12 (2023).
35. Liu, H., Li, X., Li, X. & Wang, K. Application of Hydrus-1D software in the remediation of soil hexavalent chromium contamination. *Energy Environment*, 119–122 (2024).
36. Corona, C. & Shemin, G. Examining subsurface response to an extreme precipitation event using HYDRUS-1D. *Vadose Zone J.* https://doi.org/10.1002/vzj2.20189 (2022).
37. Talat, S., Mohammad Reza, M., Majid, A., Shamsollah, A. & Daniela, S. Modeling the effect of slope aspect on temporal variation of soil water content and matric potential using different approaches by HYDRUS-1D. *Geoderma Regional* (2023). https://doi.org/10.1016/j.geodrs.2023.e00724
38. Baoqing, D. & Junye, W. Saturated-unsaturated groundwater modeling using 3D Richards equation with a coordinate transform of nonorthogonal grids. *Appl. Math. Model.* https://doi.org/10.1016/j.apm.2017.05.021 (2017).
39. Cockett, R., Heagy, L. J. & Haber, E. Efficient 3D inversions using the Richards equation. *Comput. Geosci.* **116**, 91–102 (2018).
40. Mohamed, H. Analytical solution for steady vertical flux through unsaturated soil based on Van Genuchten-Mualem model. *J. Hydrol.* https://doi.org/10.1016/j.jhydrol.2024.131066 (2024).
41. Mohamed, R., Amany, S. & Arafa, M. A modified Adam algorithm for deep neural network optimization. *Neural Comput. Appl.* https://doi.org/10.1007/s00521-023-08568-z (2023).
42. Jiří, Š., Giuseppe, B., Miroslav, Š. & Martinus Th. van, G. & The family of HYDRUS models. *Oxf. Res. Encyclopedia Environ. Sci.* https://doi.org/10.1093/acrefore/9780199389414.013.892 (2024).

Author contributions

Conceptualization was conducted by Qianxing Sun and Yanling Li. Qianxing Sun and Yanling Li developed the methodology. Formal analysis was performed by Qianxing Sun, Yanling Li, Junfang Wei, and Yuliang Fu. The original manuscript was drafted by Qianxing Sun. All authors have read and approved the final version of the manuscript.

Funding

This work was supported by the Key Scientific Research Projects Plan of Henan Higher Education Institutions (24 A120009 and 25 A570004) and the Key Science and Technology Projects in Henan Province (252102321118).

Declarations

Competing interests

The authors declare no competing interests.

Additional information

Correspondence and requests for materials should be addressed to Q.S. or Y.F.

Reprints and permissions information is available at www.nature.com/reprints.

Publisher's note Springer Nature remains neutral with regard to jurisdictional claims in published maps and institutional affiliations.